Nonlinear Modeling for 3D Weld Pool Characteristic Parameters in GTAW

Experiments have been conducted to produce random changes in the welding current and speed, resulting in fluctuations in the weld pool surface using GTAW

BY Y. K. LIU, W. J. ZHANG, AND Y. M. ZHANG

ABSTRACT

Modeling and control of the 3D weld pool surface characterized by its width, length, and convexity is an essential capability of the next generation of automated welding machines. In this paper, a nonlinear Hammerstein model is developed for the 3D weld pool surface. A real-time weld pool surface monitoring system is used to measure the specular 3D weld pool surface under a strong arc in gas tungsten arc welding (GTAW). Experiments are designed to produce random changes in the welding current and speed, resulting in fluctuations in the weld pool surface. Static modeling results suggest that the weld pool width and length can be modeled linearly, while the weld pool convexity can be better represented by a nonlinear model. Linear models for the width and length are constructed through a least-squares algorithm-based statistical analysis. A dynamic Hammerstein model is then constructed for the weld pool convexity, and the modeling results are analyzed in detail. The cross couplings between the weld pool characteristic parameters are further modeled using a neuro-fuzzy model. It is found that these nonlinear models can provide a detailed knowledge about the complex correlation between the weld pool surface and welding process inputs.

KEYWORDS

• 3D Weld Pool Surface • Nonlinear Modeling • Gas Tungsten Arc Welding (GTAW) • Hammerstein • Least Squares

Introduction

The ability to control the weld pool surface is considered an essential capability of the next generation automated welding machines (Ref. 1). It is inspired by the fact that a skilled welder can infer the weld penetration status based on his/her observation of the weld pool and control certain welding parameters accordingly. Extensive studies have been performed to observe the weld pool using various sensing techniques (Refs. 2–6), including pool oscillation, ultrasonic sensing, infrared sensing, and the vision-based sensing method. Among all types of information that can be extracted from the weld pool, the geometry of the weld pool is believed to provide valuable insights into the state of the welding process. Important information such as weld defects and weld joint penetration are contained in the surface deformation of the weld pool in gas tungsten arc welding (GTAW) (Ref. 7).

Modeling of the weld pool using the empirical method has been investigated by various researchers to some extent (Refs. 8–10). For example, Song (Ref. 8) proposed a linear discrete-time transfer function model to correlate the weld bead width and depth to the welding speed and heat input. Zhang (Ref. 9) modeled the width and depth of the weld pool using the neuro-fuzzy modeling technique. Although these methods provide some insights in modeling the weld pool width and depth/topside height, they did not characterize and model the 3D weld pool surface, which is directly visible to human welders and provides the most comprehensive information about the welding process.

Researchers have also established numerical models to analyze the correlation between the weld pool and arc/heat source (Refs. 11, 12). These models can provide detailed information about the thermal dynamics of the arc and its interactions with the weld pool, which may help understand the underlined complex correlation between the welding process inputs and weld pool. However, extensive calculations are typically required by these numerical models, which are not suitable for real-time weld pool monitoring and control applications.

Despite various studies in the past few decades, sensing and modeling of the specular and complex 3D weld pool surface remain difficult because of the following: 1) the vibration of the weld pool and strong illumination of the arc make the weld pool monitor-

Y. K. LIU, W. J. ZHANG, and Y. M. ZHANG (yuming.zhang@uky.edu) *are with the Institute for Sustainable Manufacturing and Department of Electrical and Computer Engineering, University of Kentucky, Lexington, Ky.*

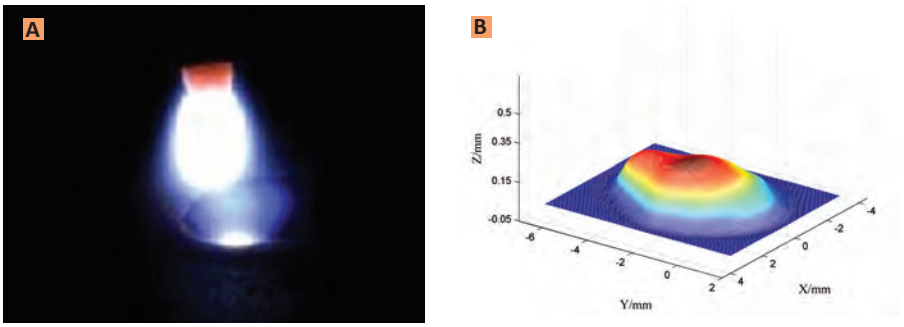

Fig. 1 — GTA weld pool. A — Pool image; B — reconstructed pool surface (Ref. 13).

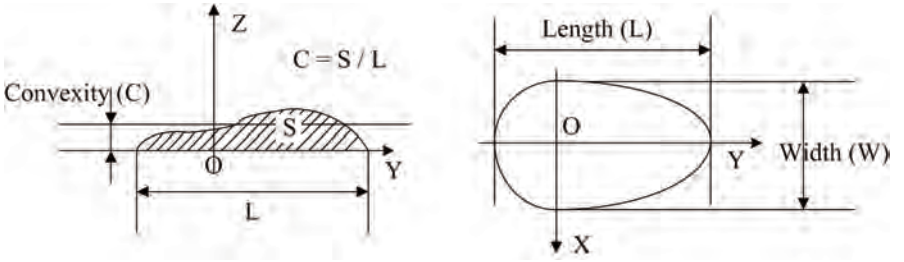

Fig. 2 — Illustration of weld pool characteristic parameters (Ref. 13).

Table 1 — Experimental and Imaging Parameters

Welding Parameters			
Current/A	Welding speed/(mm/s)	Arc length/mm	Argon flow rate/(L/min)
54–68	0.9–2.0	5	11.8
Monitoring Parameters			
Laser projection angle/deg ee		Laser to weld pool distance/mm	Imaging plane to weld pool distance/mm
35.5		24.7	101
Camera Parameters			
Shu er speed/ms		Frame rate/fps	Camera to imaging plane distance/mm
4		30	57.8

ing extremely challenging; and 2) characterizing the complex 3D weld pool point clouds is not straightforward. In the authors' previous research (Ref. 13), 3D weld pool surface is characterized by its width, length, convexity, and a steady-state correlation is found between the weld penetration specified by the back-side bead width and these characteristic parameters. Further, a dynamic model for the weld penetration is also identified under varying weld pools (Ref. 6), and it is confirmed that the proposed weld pool characteristic parameters (i.e., weld pool width, length, and convexity) are able to estimate the weld penetration with acceptable accuracy.

A linear state space model is then proposed in Ref. 1 to correlate these characteristic parameters to the welding process inputs. Although this linear model may provide some insights in understanding the relationship between inputs and weld pool characteristic parameters, the highly dynamic and nonlinear welding process cannot be comprehensively represented. The Hammerstein model, on the other hand, is considered as an effective method to model the nonlinear system (Refs. 14–16). A static input nonlinearity followed by a linear dynamical part has proven to be an adequate way to model many practical systems. In this paper, a nonlinear Hammerstein model for the 3D weld pool surface geometry characterized by its width, length, and convexity in GTAW is presented.

GTAW Process and Experimental Setup

GTAW Process

Gas tungsten arc welding is the primary process used for precision joining of metals (Ref. 17). In this process, an arc is established between the nonconsumable tungsten electrode and the base metal. The base metal is melted by the arc and forms a liquid weld pool that joins the two pieces of the base metal together after solidification. The shielding gas is fed through the torch to protect the electrode, molten weld pool, and solidifying weld metal from contamination by the surrounding atmosphere. Filler is typically needed to finish the weld. However, for the most critical root pass where complete joint penetration is concerned, filler is typically optional. This work focuses on the root pass without filler metal.

The weld pool is the core of the welding process where the complex phenomenon originates. The weld pool geometry may provide valuable insights into the state of the welding process (see Fig. 1A and B for a weld pool image and reconstructed weld pool surface using an image processing and reconstruction algorithm detailed in Ref. 4). Yet the 3D point clouds of the weld pool shape are large and impractical to use in real-time weld pool control applications.

Figure 2 presents the characterization parameters of the 3D weld pool geometry proposed in Ref. 13. The characterization parameters include the following: width (W), length (L), and convexity (C) of the weld pool. Specifically, the convexity is defined as the average height of the weld pool along the longitude direction, i.e., the total area above the workpiece (S) divided by the length L (shown in Fig. 2 left). These parameters will be used as the outputs of the system. Among all the welding process inputs, an increase in the welding current and a decrease in the welding speed will significantly increase the heat input into the welding process, thus influencing the weld pool surface geometry considerably. The GTAW process is defined as a two-input-three-output system, with the welding current and speed as its

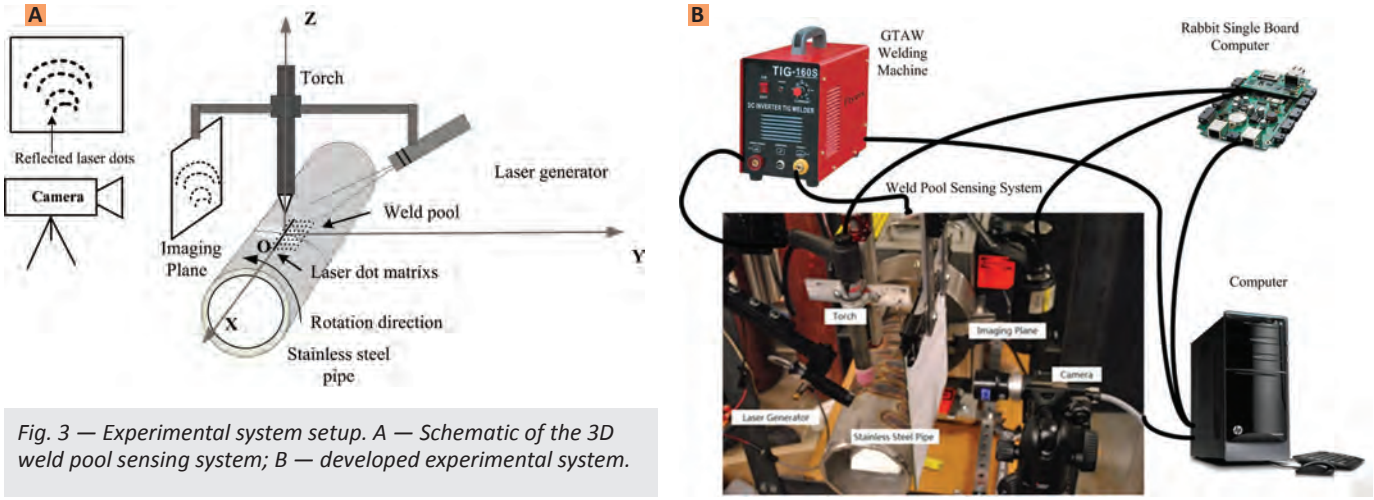

Fig. 3 — Experimental system setup. A — Schematic of the 3D weld pool sensing system; B — developed experimental system.

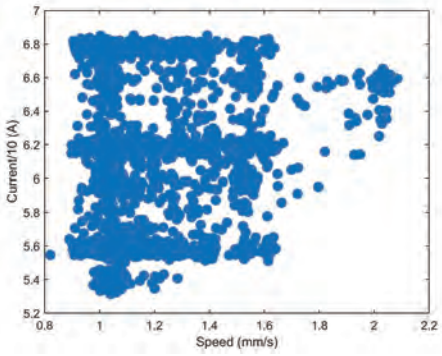

Fig. 4 — Distribution of welding current and speed in 13 dynamic experiments.

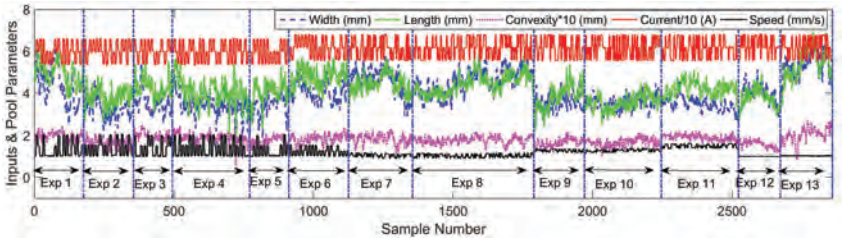

Fig. 5 — Measured data in 13 dynamic experiments.

inputs, and the weld pool characteristic parameters including the pool width, length, and convexity as its outputs.

Experimental System

In this subsection, the experimental system used in this study is briefly reviewed. The experimental setup is illustrated in Fig. 3, including a recently developed 3D weld pool sensing system detailed in Ref. 21. Specifically, a 20-mW illumination laser generator is used to project a 19 by 19 dot matrix structured light pattern on the weld pool region — Fig. 3A. Part of the dot matrix projected inside the weld pool is reflected by the specular weld pool surface, which is depressed and distorted. This distortion of the reflected dot matrix is determined by the shape of the three-dimensional weld pool surface and contains the 3D geometry information about the weld pool. This approach makes use of a relatively simple idea to facilitate a practical solution to overcome the two challenges (bright arc and specular surface) aforementioned: By exploiting the propagation difference between laser and plasma, the laser rays mirrored from the weld pool surface can be clearly imaged in the presence of bright plasma, thus changing the specular surface from a difficulty to an advantage.

Table 2 — Model Order Selectio

	Previous Measurements Order	Welding Current Order	Welding Speed Order
Width	2	2	3
Length	2	3	6
Convexity	2	3	3

More specifically, the reflected laser keeps straight travel without significant loss of intensity over distance while the radiation of the arc energy decays rapidly over distance. By using specific image processing and the reconstruction algorithm detailed in Ref. 21, the 3D weld pool characteristic parameters can be measured in real time.

An imaging plane is installed with a distance of about 100 mm from the torch. A camera is located behind the imaging plane. The welds are made using direct-current electrode-negative GTAW. The material of the pipe is stainless steel 304. The outer diameter and wall thickness of the pipe are 113.5 and 2.03 mm, respectively. The pipe rotates during experiments while the positions of the torch, imaging plane, laser structure light generator, and camera are stationary.

The images captured by the camera are transferred to a computer where the images are processed, the 3D weld pool surfaces are reconstructed, and the weld pool characteristic parameters are calculated. To validate the proposed sensing system, in Ref. 20 a spherical mirror with known geometry is utilized to validate the accuracy of the 3D weld pool surface reconstruction algorithm. Slags floating on the weld pool surface would block the laser pattern from being reflected and thus negatively affect our proposed 3D weld pool sensing system.

Fortunately, for our algorithm, the missing reflection from some projected

laser dots would not affect the ability to reconstruct the weld pool surface because the reflection dots are redundant. To avoid the possibility of a large area of slag, the workpiece surface was ensured to be rustfree. The rotation speed and motion of the torch are controlled by a Rabbit single board computer to achieve the required welding speed and arc length. The welding current is controlled by the computer through its analog output to the power supply.

Experiment Design

Thirteen dynamic experiments were conducted as bead-on-plate welding, with the welding parameters and imaging parameters specified in Table 1. The sampling time in this study was 0.33 s. Welding current was randomly changed through all 13 experiments, while the welding speed was considerably varied in experiments 1 to 6, moderately varied in experiments 7 to 11, and remained constant in experiments 12 and 13. Each experiment lasted from about 50 to 120 s, resulting in roughly 150 to 400 data points.

Figure 4 shows the distribution of the welding current and speed in these dynamic experiments. This distribution implies that the resultant model can be used during control if the welding current and speed are in the range specified by this distribution.

Figure 5 plots the inputs and measured weld pool characteristic parameters in all 13 experiments. The pool parameters are measured at 30 Hz and averaged over the interval to provide smooth measurements. It is observed that the weld pool varies substantially resulting from fluctuations in the welding current and speed. Specifically, the ranges for the weld pool width, length, and convexity are [1, 6.42 mm], [1.2, 6.9 mm], and [0.05, 0.27 mm], respectively.

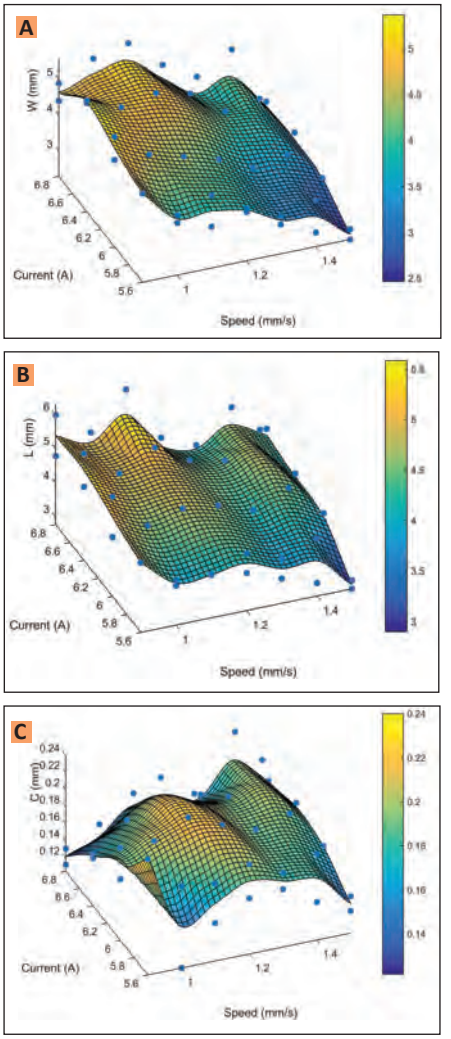

Fig. 6 — Static response. A — Width; B — length; C — convexity.

Static Nonlinearity

The welding process is generally considered to be dynamic and nonlinear. To examine the static nonlinear correlation between the system outputs (weld pool width, length, and convexity) and inputs (welding current and speed), 55 static experiments were carried out prior to the 13 dynamic experiments shown in Fig. 5. In these experiments, the welding current was from 56 to 68 A, and the welding speed ranged from 0.9 to 1.5 mm/s, but kept constant during each experiment. The empirical static correlations obtained from these static experiments are shown in Fig. 6.

It is observed in Fig. 6A that the weld pool width is roughly linearly correlated to the welding current and speed. As the welding current becomes larger (or welding speed becomes smaller), the width becomes larger.

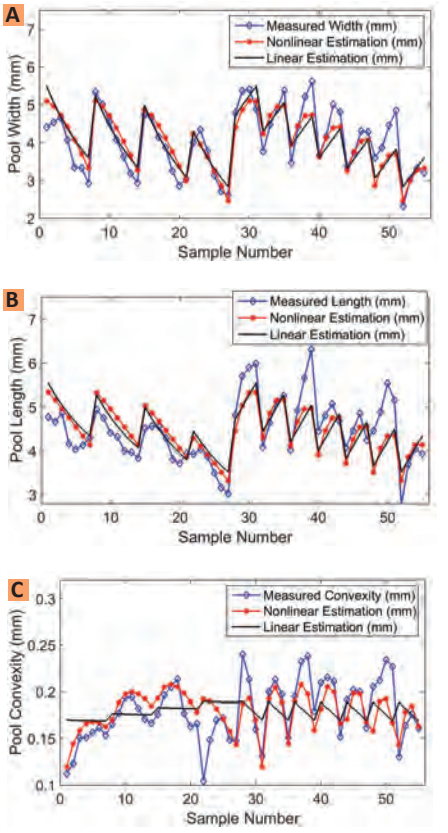

Fig. 7 — Linear and nonlinear static response model fitting results. A — Width; B — length; C — convexity.

Table 3 — Model Parameters

	Previous Measurement α_w, α_L, α_{cl}, α_c	Welding current β_w, β_L, β_{cl}, β_c (mm/A)	Welding speed γ_w, γ_L, γ_{cl}, γ_c (mm$\sqrt{mm/s}$)	Constant c_w, c_L, c_{cl}, c_c (mm)
Width	[0.802 0.099]	[0.19 –0.054]	[0.029 0.386 0.131]	–0.941
Length	[0.708 0.187]	[0.06 –0.01 0.001]	[–0.039 –0.581 0.416 –0.338 0.516 –0.041]	0.231
Convexity (Linear)	[0.582 0.221]	[0.017 0.035 –0.006]	[–0.001 0.053 –0.002]	0.034
Convexity (Nonlinear)	[0.584 0.201]	[–0.006 0.002 0.001]	[–0.014 –0.001 0.012]	0.071

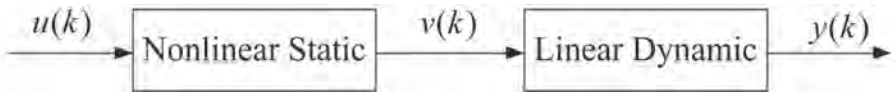

Fig. 8 — Hammerstein model.

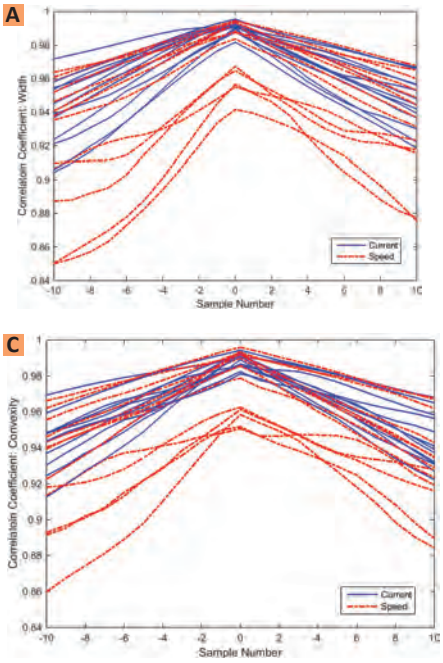

Fig. 9 — Cross correlation analysis. A — Width; B — length; C — convexity.

This makes sense because an increase in the welding current (or decrease in the welding speed) should cause heat input and thus the overall pool size and weld pool width to increase. The weld pool length also appears to be roughly linearly correlated to the current and welding speed — Fig. 6B. An increase in the welding speed or a decrease in the welding current would result in a decrease in the weld pool length. This is understandable since a reduced heat input would decrease the volume of the melted metal and weld pool length.

Figure 6C shows a highly nonlinear correlation between the weld pool convexity and welding process inputs. For low welding speeds, an increase in the welding current causes a decrease in the weld pool convexity. In this case, the complete joint penetration is achieved. As the welding current increases, the arc pressure acting on the weld pool becomes larger, and the weld pool becomes less convex, which makes the convexity smaller. While for moderate welding speeds, the convexity will first increase, then decrease given an increase in the welding current. This makes sense because when the current is relatively small, only partial penetration is achieved, and an increasing current should increase the amount of metals to be melted and thus the convexity.

As the current becomes larger, complete joint penetration occurs, and the convexity becomes smaller due to larger arc pressure and penetration capability. For high welding speeds, the pool convexity generally increases as the current increases. In this case, partial penetration occurs and the sufficiency of the heat input becomes the major factor in determining the convexity. An increase in the welding current should increase the heat input and the amount of metal melted, and the weld pool convexity would increase accordingly.

The above analysis reveals the complex static correlation between the pool parameters and welding process inputs. The Hammerstein model (shown in Fig. 8) has been considered as an effective method to model the nonlinear systems (Refs. 14–16). A static input nonlinearity followed by a linear dynamical part has proven to be an adequate way to model many nonlinear systems. In our study, $u(k) = [u_1(k), u_2(k)]$, where $u_1 = I = i/10$ and $u_2 = 1/\sqrt{S}$ with i as the welding current and S as the traveling speed.

The heat input of the arc in a unit interval along the travel direction can be written as a nonlinear function of I^2 and 1/S:

$$\Delta H \propto f\ (I^2,\ 1/S) \qquad (1)$$

Roughly speaking, one can assume that the volume of the weld pool, thus also the volume of the 3D weld pool surface due to thermal expansion, is approximately proportional to the heat input. By characterizing the 3D weld pool surface using its width, length, and convexity, a linear model structure may be expressed as follows

$$[W,\ L,\ C]\ \propto g\ (I,\ 1/\sqrt{S}) \qquad (2)$$

where g's are linear functions of the current and square root of the reciprocal of welding speed.

The static linear model fitting results are illustrated in Fig. 7. As can be seen, linear models are not sufficient in representing this correlation, and large fitting errors are frequently observed. Such fitting errors may be reduced when nonlinear static models are used. Modeling trials suggest the following nonlinear function structure provides a good estimation

$$[W,\ L,\ C]\ \propto h\ (I^2,\ I,\ 1/S,\ 1/\sqrt{S},\ I/\sqrt{S}) \qquad (3)$$

It is noticed that although the above model (3) is nonlinear with respect to the welding current and welding speed, the model is still linear in parameters, and thus can be identified using the standard least-squares method. The nonlinear model fitting results are plotted in Fig. 7. It is observed that for the width and length, incorporating nonlinearity does not improve the fitting results significantly.

It is noted, however, that certain static modeling errors exist for the weld pool width and length (for example in samples numbered 38, 39, 42, 43, and 48–51). This is primarily due to unmodeled factors during the extremely com-

Table 4 — Model Errors

	E_{ave} (mm)	RMSE (mm)
Width	0.1797	0.2326
Length	0.2218	0.2929
Convexity (Linear)	0.0121	0.0158
Convexity (Nonlinear)	0.0114	0.0147

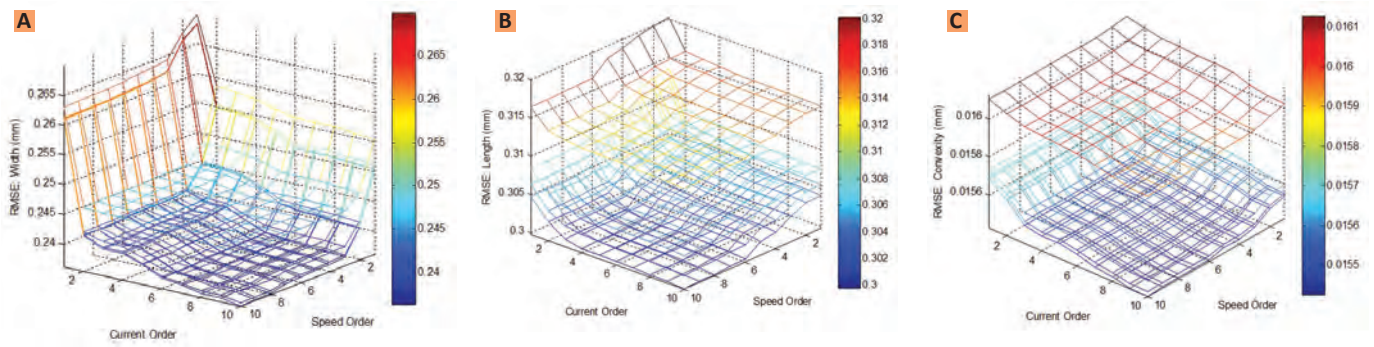

Fig. 10 — Order selection with respect to RMSE. A — Width; B — length; C — convexity.

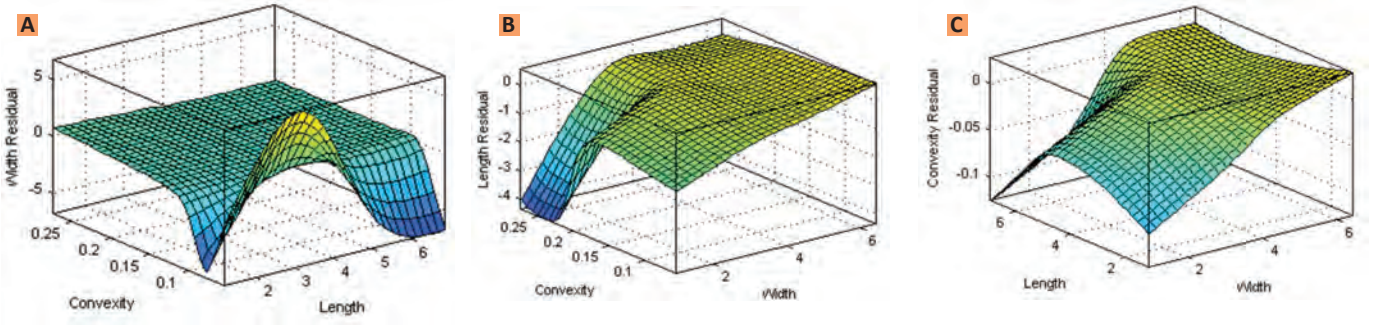

Fig. 11 — Cross-correlation modeling surface. A — Width; B — length; C — convexity.

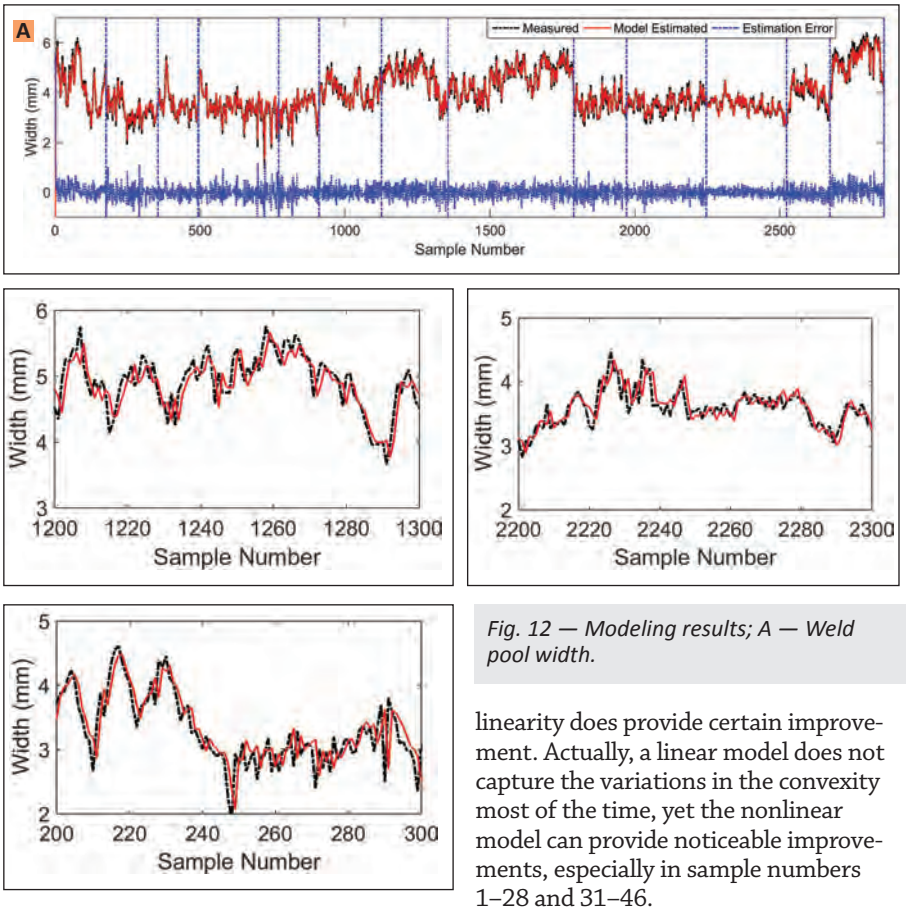

Fig. 12 — Modeling results; A — Weld pool width.

plex and dynamic welding processes. For the convexity, introducing the nonlinearity does provide certain improvement. Actually, a linear model does not capture the variations in the convexity most of the time, yet the nonlinear model can provide noticeable improvements, especially in sample numbers 1–28 and 31–46.

The width and length will be modeled using dynamic linear models, and the convexity will be modeled using the nonlinear Hammerstein model. The identified nonlinear static model for the convexity is

$$C_n = 1.36I - 0.09I^2 + 4.75/\sqrt{S} - 1.53/S - 0.31I/\sqrt{S} - 6.17 \quad (4)$$

The affined inputs can be defined as

$$v_1 = 1.36I - 0.09I^2 - 0.31I/\sqrt{S} \quad (5A)$$

$$v_2 = 4.75/\sqrt{S} - 1.53/S - 6.17 \quad (5B)$$

In the next section, the affined inputs, Equations 5A and B, will be used as the input to the linear dynamic model.

Dynamic Modeling

Cross-Correlation Analysis

Cross-correlation analysis between the outputs (weld pool width, length, and convexity) and welding process inputs (welding current and speed) is first performed to examine possible delays in the system (Ref. 18).

Figure 9 illustrates the cross-correlation between the inputs and

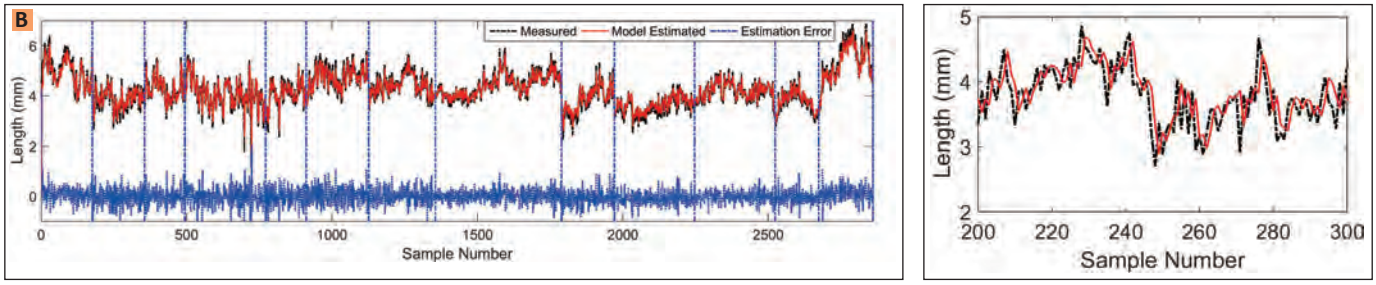

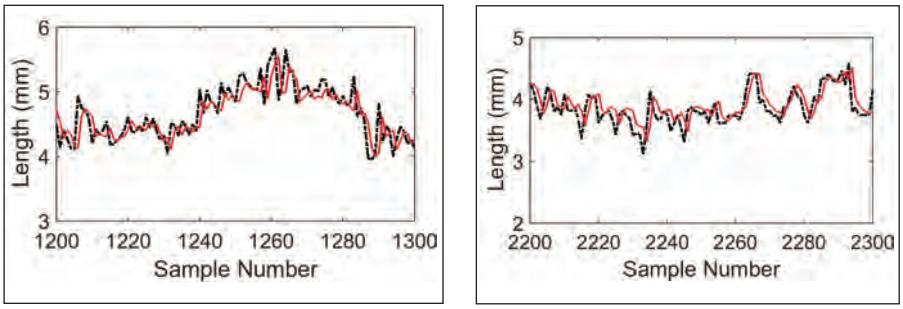

Fig. 12 — Modeling results; B — length.

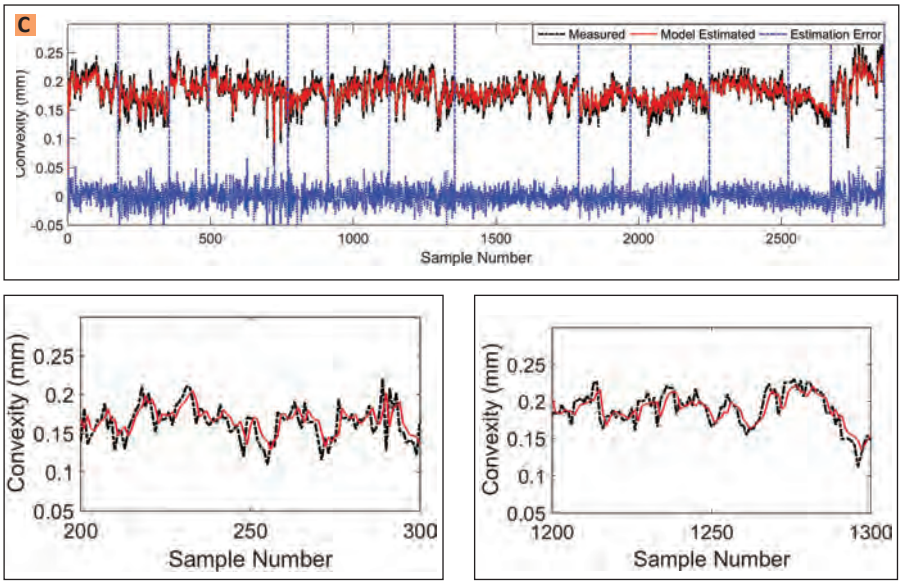

Fig. 12 — Modeling results; C — convexity.

outputs for all 13 dynamic experiments. It is observed that although the correlation coefficients vary from individual experiments, there is no delay for the width, length, and convexity with respect to the welding process inputs. Thus, the model structures can be expressed as

$$W(k)=\sum_{j=1}^{n_{w,w}}\alpha_W(j)W(k-j)+\sum_{j=1}^{n_{w,i}}\beta_W(j)u_1(k-j)+\sum_{j=1}^{n_{w,s}}\gamma_W(j)u_2(k-j)+c_W \quad (6A)$$

$$L(k)=\sum_{j=1}^{n_{L,L}}\alpha_L(j)L(k-j)+\sum_{j=1}^{n_{L,i}}\beta_L(j)u_1(k-j)+\sum_{j=1}^{n_{w,s}}\gamma_L(j)u_2(k-j)+c_L \quad (6B)$$

$$C(k)=\sum_{j=1}^{n_{C,C}}\alpha_C(j)C(k-j)+\sum_{j=1}^{n_{C,i}}\beta_C(j)v_1(k-j)+\sum_{j=1}^{n_{C,s}}\gamma_C(j)v_2(k-j)+c_C \quad (6C)$$

where W(k–j), L(k–j), C(k–j) are the weld pool width, length, and convexity at instant k–j, $n_{w,w}$, $n_{w,i}$, $n_{w,s}$ are the orders for the width and $\alpha_W(j)$, $\beta_W(j)$, $\gamma_W(j)$, c_W are the parameters for the width model to be identified. Model orders and parameters for the length and convexity models can be similarly defined.

The linear model for the convexity can also be expressed as

$$C(k)=\sum_{j=1}^{n_{C,C}}\alpha_{Cl}(j)C(k-j)+\sum_{j=1}^{n_{C,i}}\beta_{Cl}(j)u_1(k-j)+\sum_{j=1}^{n_{C,s}}\gamma_{Cl}(j)u_2(k-j)+C_{Cl} \quad (7)$$

where $\alpha_{Cl}(j)$, $\beta_{Cl}(j)$, $\gamma_{Cl}(j)$, and c_{Cl} are the linear model parameters.

Order Selection

The following two criteria are proposed to evaluate the performance of the developed linear and Hammerstein models.

The model average error is defined by

$$E_{ave}=\frac{1}{N}\sum_{k=1}^{N}|\hat{y}(k)-y(k)| \quad (8)$$

where N is the number of samples, $\hat{y}$ is the estimated system output (weld pool width, length, and convexity in this study) by the proposed model, and y is the measured system output.

The root mean square error (RMSE) of the model is calculated by

$$RMSE=\sqrt{\sum_{k=1}^{N}(\hat{y}(k)-y(k))^2/N} \quad (9)$$

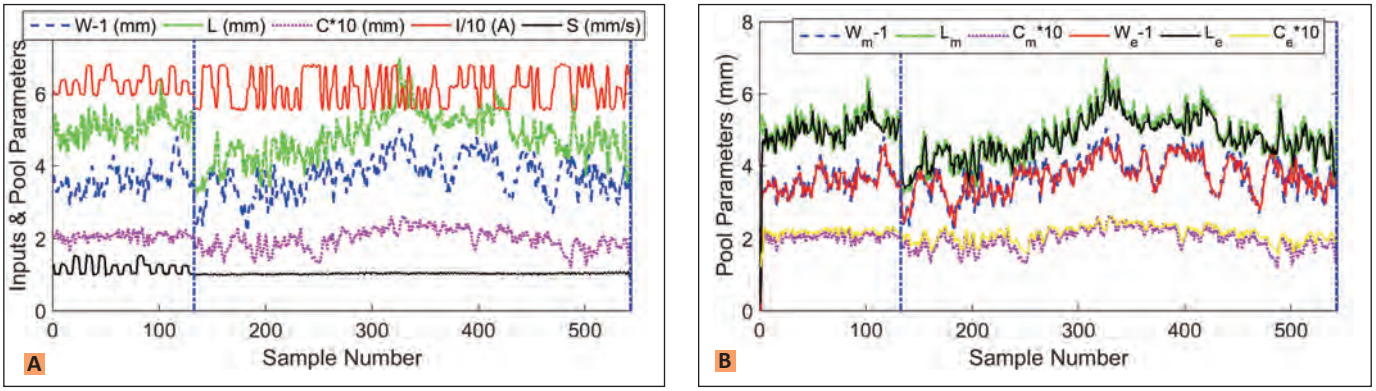

Fig. 13 — Model verification experiments results. A — Measured welding process inputs (welding current and speed) and outputs (weld pool width, length, and convexity); B — model estimated weld pool characteristic parameters.

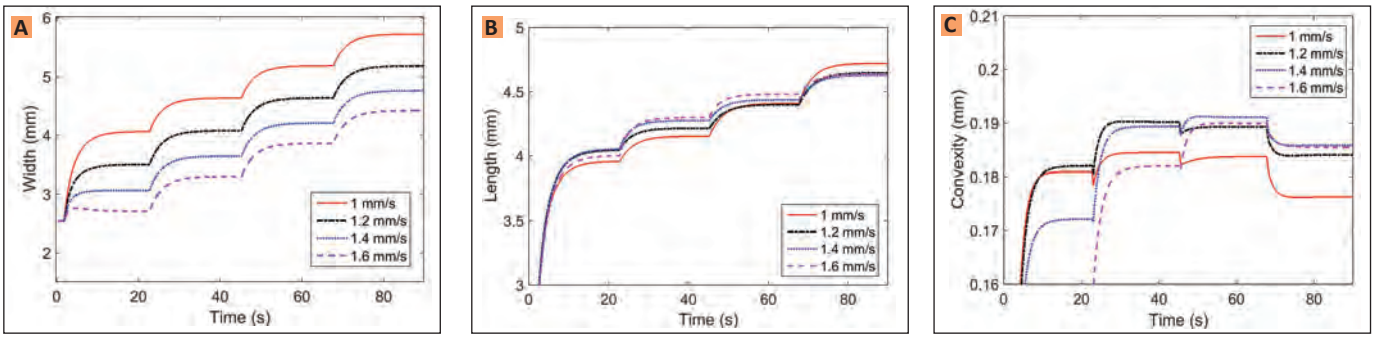

Fig. 14 — Model estimated weld pool parameters at varying welding currents and speeds. A — Width; B — length; C — convexity.

The model orders are selected based on evaluating the RMSE defined in Equation 9 and is visualized in Fig. 10. For the width (Fig. 10A), RMSE surfaces using up to four previous width measurements are plotted, with $n_{w,w}$ = 1, 2, 3, 4 corresponding to each plane from top to bottom. It is observed that when $n_{w,w}$ is larger than 2, the differences in RMSE becomes negligible. In this sense, $n_{w,w}$ = 2 is selected. Similarly, the order of the welding current and speed can be determined.

For the weld pool length and convexity, an identical procedure can be employed and the full set of model orders is listed in Table 2. It is noticed that the statistical-based method may also be employed to determine the model order, such as the F test. However, to perform the F test, we would have to generate a three-dimension table (with each dimension corresponding to the model inputs, including the previous measurements, welding current, and the square root of the reciprocal of the welding speed), which is hard to interpret and visualize. By visualizing the RMSE for the width, length, and convexity, on the other hand, the trends of the errors with respect to the model orders are directly observed.

Modeling the Cross-Coupling between Pool Parameters

Models 6A–C can capture the dynamic correlations between the welding process inputs and outputs. However, pool parameters may also be coupled. The neuro-fuzzy technique (Ref. 19) may be utilized to model the residuals with other two pool parameters at the current instant. The corresponding models are finally expressed as

$$W(k)=\sum_{j=1}^{n_{w,w}}\alpha_W(j)W(k-j)+\sum_{j=1}^{n_{w,i}}\beta_W(j)u_1(k-j)+\sum_{j=1}^{n_{w,s}}\gamma_W(j)u_2(k-j)+c_W+NFW \quad (10A)$$

$$L(k)=\sum_{j=1}^{n_{L,L}}\alpha_L(j)L(k-i)+\sum_{j=1}^{n_{L,i}}\beta_L(j)u_1(k-j)+\sum_{j=1}^{n_{w,s}}\gamma_L(j)u_2(k-j)+c_L+NFL \quad (10B)$$

$$C(k)=\sum_{j=1}^{n_{C,C}}\alpha_C(j)C(k-j)+\sum_{j=1}^{n_{C,i}}\beta_C(j)v_1(k-j)+\sum_{j=1}^{n_{C,s}}\gamma_C(j)v_2(k-j)+c_C+NFC \quad (10C)$$

where NFW, NFL, and NFC represent the residuals for the width, length, and convexity correlated by the neuro-fuzzy model.

The modeling surfaces for residuals of the width, length, and convexity are shown in Fig. 11. Take convexity residual, for example (Fig. 11C), when the width and length are both small, the convexity residual tends to be small. This makes sense because small width/length indicates insufficient heat input and metals that are melted, so the convexity residual is small. Modeling results are shown in the next subsection.

Modeling Result

The linear modeling results for the width and length are plotted in Fig. 12A, B, and the nonlinear modeling result for the convexity is depicted in Fig. 12C. The identified dynamic model parameters for Equations 10A–C and 7 are listed in Table 3.

For the weld pool width, the coefficients for the previous width measurements at k–1 and k–2 instants are 0.802 and 0.099, respectively. The measurement at k–1 instant contributes more than that at k–2 instant. The coefficients for the welding current input are 0.19 and –0.054, indicating an overall positive correlation. These dynamic model parameters could help understand the detailed relationship between the inputs and weld pool parameters. More importantly, these parameters can also derive steady-state models for the weld pool width, length, and convexity, which will be analyzed in the model analysis section.

The obtained model errors are shown in Table 4. Specifically, the calculated average model error and RMSE for the width are 0.1797 and 0.2326 mm, respectively. The calculated average model error and RMSE for the length are 0.2218 and 0.2929 mm, respectively. The calculated average model error and RMSE for the nonlinear Hammerstein convexity model are 0.0114 and 0.0147 mm, respectively. For the linear convexity model, the calculated average model error and RMSE are 0.0121 and 0.0158 mm, respectively. It is observed that the proposed model is able to correlate the dynamic relationship between the weld pool state and welding process inputs with acceptable accuracy. Comparing the linear convexity model and nonlinear Hammerstein model, both the average model error and RMSE are improved by 6%. It is concluded that the nonlinear model with cross coupling can better represent the dynamic and nonlinear weld pool convexity. Detailed model analysis will be discussed in the model analysis section.

Model Verification

To validate the proposed dynamic linear model, two validation experiments are carried out. The inputs and measured front-side weld pool characteristic parameters are plotted in Fig. 13A. In experiment 1, both the welding current and welding speed are varied randomly in a range of [60, 70 A] and [1, 1.5 mm/s], respectively. In experiment 2, the welding current is randomly changed from 55 to 70 A, while the welding speed is 1 mm/s during the experiment. Other experimental parameters are the same as those listed in Table 1.

It is observed that in both experiments the weld pool width and length increase with an increase in the welding current, and the convexity decreases, indicating a more depressed weld pool. Figure 13B plots the measured weld pool characteristic parameters and estimated values by the dynamic linear model. It is observed that the weld pool parameters can be estimated with acceptable accuracy using the obtained models in models 6A–C. Specifically, the average model error for the width, length, and convexity is 0.2028, 0.2637, and 0.0348 mm, respectively. The RMSE for the width, length, and convexity is 0.2565, 0.3444, and 0.0374 mm, respectively.

Model Analysis

The identified models can be used to analyze the process. We first use identified linear models since the linear models as an average model over the entire input range can represent the correlation with certain accuracy.

The steady-state models for the width, length, and convexity can be derived from Equations 6A–C together with parameters specified in Table 3.

$$W = 1.36I + 5.46/\sqrt{S} - 9.41 \quad (11A)$$

$$L = 0.486I - 0.638/\sqrt{S} + 2.2 \quad (11B)$$

$$C = -0.0152I - 0.0152/\sqrt{S} + 0.3604 \quad (11C)$$

For the weld pool width, the static gain for I and $1/\sqrt{S}$ is 1.36 mm/A and 5.46 mm$\sqrt{\text{mm/s}}$, respectively. The positive gains make sense because an increase in the welding current and a decrease in the welding speed (thus an increase in $1/\sqrt{S}$) both increase the heat input into the weld pool. The width of the pool is likely to increase. For the weld pool length, it also increases when increasing the welding current (thus the heat input).

However, the increasing rate is less significant than the width (0.486 mm/A compared to 1.36 mm/A). When the welding speed decreases, the length decreases with a negative coefficient –0.638 mm$\sqrt{\text{mm/s}}$. This is because an increased speed tends to elongate the weld pool. In this sense, this small negative coefficient is actually a combination of two contradictory effects (decreasing heat input but elongating the pool). For the convexity, increasing the welding current and decreasing the welding speed cause a decrease in the weld pool convexity with both coefficients being –0.0152 mm/A and –0.0152 mm$\sqrt{\text{mm/s}}$.

It is because increasing welding current and decreasing welding speed both increase the heat input to increase the joint penetration. It is also because the arc pressure increases as the current increases. For complete joint penetration, the concavity of the weld pool surface increases as the penetration and arc pressure increase. Therefore, the convexity reduces.

However, as the static response (in Fig. 6) indicates, the relationships between the weld pool convexity and inputs are highly nonlinear. The linear model (11C) might not be sufficient in understanding this complex nonlinear relationship. Figure 14 plots the model calculated width, length, and convexity for four cases of welding speeds (1, 1.2, 1.4, and 1.6 mm/s) when the welding current increases from 56 to 60 A, 64 and 68 A. As the welding current increases, the width also increases. For a given welding current, increasing the welding speed decreases the weld pool width. This coincides with our analysis from the steady-state model (11A). The settling time for the width is roughly 4 s, which agrees with steady-state experimental results. For the weld pool length, as the current increases, it becomes longer. For a given welding current, increasing the welding speed increases the weld pool length.

The nonlinear correlations between the convexity and welding process inputs are depicted in Fig. 14C. For a low welding speed (i.e., 1 mm/s), as the welding current increases, the pool con-

vexity first increases, then starts to decrease. Actually when the current increases, more metals are melted, resulting in greater convexity. However, as the current increases, the increase in the arc pressure becomes the dominant factor. The pool becomes more concave and the penetration becomes deeper. Thus, the pool convexity starts to decrease.

Similar phenomena occur for other welding speeds, while the dominant factor might be different for different welding currents. The increasing rates for different welding speeds are also different as opposed to the linear models for the width and length (shown in Fig. 14A and B). It is apparent that the above observations provide us detailed knowledge about the correlations between the weld pool geometry and welding current/speed. They are derived from the nonlinear Hammerstein model. If a linear model is used, the correlation acquired between the weld pool geometrical parameters and process inputs will only be an average over the entire range of the inputs. The above observations cannot be drawn. Hence, the nonlinear model plays an important role in accurately modeling the weld pool geometry and understanding this complex correlation.

Conclusion

The ability to control the 3D weld pool surface is considered as a key capability of the next generation of automated welding machines. A first yet essential step toward such ability is to accurately model the 3D weld pool surface characterized by its width, length, and convexity. In this paper, dynamic experiments have been conducted to produce random changes in the welding current and speed, resulting in fluctuations in the weld pool surface using GTAW. Linear models for the width and length are constructed through least-squares algorithm. The nonlinear dynamic Hammerstein model for the weld pool convexity is then constructed to improve the modeling performance, and the results are analyzed in detail. It is found from the derived steady-state model that the weld pool width and length is positively correlated to the welding current, yet the convexity is negatively correlated to the welding current.

The identified dynamic models further provide us detailed knowledge about the correlations between the weld pool geometry and welding current/speed. These models are essential to understanding such complex correlations and accurately controlling the welding processes. In the future, this nonlinear model-based closed-loop control system will be developed to accurately control the weld pool surface in GTAW process. Further, the models are identified using data from experiments. While the modeling methods used and the model structures may be extended to other materials under different experimental conditions, cautions must be exercised and the model parameters must be identified from experiments representing the intended applications.

Acknowledgment

This work was funded by the National Science Foundation under grant CMMI-0927707 and IIS-1208420.

References

1. Liu, Y. K., and Zhang, Y. M. 2013. Control of 3D weld pool surface. *Control Engineering Practice* 21(11): 1469–1480.

2. Rokhlin, S. I., and Guu, A. C. 1993. A study of arc force, pool depression, and weld penetration during gas tungsten arc welding. *Welding Journal* 72(8): 381–390.

3. Balfour, C., Smith, J. S., and Al-Shamma´a, A. I. 2006. A novel edge feature correlation algorithm for real-time computer vision-based molten weld pool measurements. *Welding Journal* 85(1): 1–8.

4. Song, H. S., and Zhang, Y. M. 2009. Error analysis of a three-dimensional GTA weld pool surface measurement system. *Welding Journal* 88(7): 141–148.

5. Ma, H. B., and Wei, S. C. 2010. Binocular vision system for both weld pool and root gap in robot welding process. *Sensor Review* 30(2): 116–123.

6. Liu, Y. K., Zhang, W. J., and Zhang, Y. M. 2013. Estimation of weld joint penetration under varying GTA pools. *Welding Journal* 92(11): 313-s to 321-s.

7. Liu, Y. K., and Zhang, Y. M. 2014. Model-based predictive control of weld penetration in gas tungsten arc welding. *IEEE Transactions on Control Systems Technology* 22(3): 955–966.

8. Song, J. B., and Hardt, D. E. 1994. Dynamic modeling and adaptive control of the gas metal arc welding process. *ASME Journal of Dynamics Systems, Measurement, and Control* 116(3): 405–410.

9. Zhang, Y. M., and Kovacevic, R. 1998. Neuro-fuzzy model-based predictive control of weld fusion zone geometry. *IEEE Transactions on Fuzzy Systems* 6(3): 389–401.

10. Zhang, G. J., Chen, S. B., and Wu, L. 2005. Intelligent control of pulsed GTAW with filter metal. *Welding Journal* 84(1): 9-s to 16-s.

11. Traidia, A., and Roger, F. 2011. Numerical and experimental study of arc and weld pool behaviour for pulsed current GTA welding. *Int. J. Heat Mass Transfer* 54: 2163–2179.

12. Mougenot, J., Gonzalez, J.-J., Freton, P., and Masquere, M. 2013. Plasma–weld pool interaction in tungsten inert-gas configuration. *J. Phys. D: Appl. Phys.* 46: 135206.

13. Zhang, W. J., Liu, Y. K., Wang, X., and Zhang, Y. M. 2012. Characterization of three-dimensional weld pool surface in gas tungsten arc welding. *Welding Journal* 91(7): 195-s to 203-s.

14. Cai, Z., and Bai, E.-W. 2011. Making parametric Hammerstein system identification a linear problem. *Automatica* 47(8): 1806–1812.

15. Liu, Y., and Bai, E.-W. 2007. Iterative identification of Hammerstein systems. *Automatica* 43(2): 346–354.

16. Zhao, W. X. 2010. Parametric identification of Hammerstein systems with consistency results using stochastic inputs. *IEEE Transactions on Automatic Control* 55(2): 474–480.

17. O'Brien, R., ed. 1998. Welding processes. AWS, Vol. 2, 8th ed. Miami, Fla.

18. Billings, S. A. 2013. *Nonlinear System Identification: NARMAX Methods in the Time, Frequency, and Spatio-Temporal Domains*. Wiley.

19. Liu, Y. K., Zhang, W. J., and Zhang, Y. M. 2015. Dynamic neuro-fuzzy based human intelligence modeling and control in GTAW. *IEEE Transactions on Automation Science and Engineering*, 12(1): 324–335.

20. Zhang, W. J., Liu, Y. K., and Zhang, Y. M. 2012. *Real-Time Measurement of Three Dimensional Weld Pool Surface in GTAW*. Welding Process, InTech. ISBN 979-953-307-1089-4.

21. Zhang, W. J., Wang, X. W., and Zhang, Y. M. 2013. Analytical real-time measurement of three dimensional specular weld pool surface. *Measurement Science and Technology* 24(11).